Measurement of a photonic waveguide group index via interferometry

christopher_phenicie

I. Introduction

In this work, we will measure the group index of a silicon photonic waveguide taking advantage of high-sensitivity interferometry. The proposed chip will contain a total of seven interferometers. With a proper understanding of the transfer function of an interferometer as the length imbalance of the two legs (ΔL) is changed, it is possible to make a careful measurement of the group index of the waveguides the interferometer is composed of. The proposed chip will include two different interferometer geometries, Mach-Zehnder interferometers (MZIs) to make measurements for relatively small imbalances ($\Delta \mathrm{L} \sim 100\mu$m), and Michelson interferometers (MIs) to make meausurements for relatively large imbalances ($\Delta \mathrm{L} > 1$ mm). We choose to work with MIs for this application because the geometry allows for longer length imbalances given the same amount of space on a chip. These interferometers will be sensitive to small changes in the group index due to fabrication imperfections, and we can bound the fabrication imperfections based on the observed variations in the transfer function.

II. Theory

The group index of a material can be measured from the transfer function of an unbalanced interferometer of known length difference ΔL. Let us consider the case of an interferometer composed of lossless Si photonic waveguides. As described in [1], an MZI can be built on a silicon photonic chip using two Y-branches, one as a splitter to split the incoming light between two waveguides of length L_1 and L_2, and the other Y-branch used as a coupler to allow the light to interfere. We can describe the power measured at the output of the interferometer as follows:

First, the incoming light described by the electric field E_i is split into the two branches of the Y-branch equally, meaning the field into the two waveguides are $E_1 = E_2 = \frac{E_i}{\sqrt{2}}$. These fields are then propagated along the waveguides, which have effective index n_1 and n_2 and lengths L_1 and L_2 respectively. Therefore, the fields at the opposite end of the waveguides are $E_{o1} = \frac{E_i}{\sqrt{2}} e^{-i\beta_1 L_1}$ and $E_{o2} = \frac{E_i}{\sqrt{2}} e^{-i\beta_2 L_2}$ where we define the propagation constant

$$\beta = \frac{2\pi n}{\lambda} \tag{1}$$

where n is the (effective) index of refraction of the waveguide, and λ is the wavelength of the light.

The combining Y-branch will then mix these two fields, producing the output field

$$E_o = \frac{E_{o1} + E_{o2}}{\sqrt{2}} = \frac{E_i}{2}\left(e^{-i\beta_1 L_1} + e^{-i\beta_2 L_2}\right) \tag{2}$$

In these experiments, we will only consider the intensity of the output light $I_o = |E_o|^2$, which can be simplified to the final equation which we will refer to as the transfer function of the MZI:

$$I_o/I_i = \frac{1}{2}(1 + \cos(\beta_1 L_1 - \beta_2 L_2)) \tag{3}$$

For now, we will assume that the waveguides are made of identical material, such that $\beta_1 = \beta_2 = \frac{2\pi n_{\text{eff}}}{\lambda}$ where n_{eff} is the effective index of the waveguide. Then, defining the difference in the path lengths of the two legs of the interferometer $\Delta L = L_2 - L_1$, we arrive at the following equation for the tranfer function of the imbalanced MZI with waveguides made of identical material:

$$\frac{I_o}{I_i} = \frac{1}{2}\left(1 + \cos(\beta \Delta_L)\right) = \frac{1}{2}\left(1 + \cos\left(\frac{2\pi n_{\text{eff}} \Delta_L}{\lambda}\right)\right) \tag{4}$$

Note that this is a periodic function that varies with the wavelength of the light λ. So, if we take a spectrum of this device, that is, measure I_o for a range of different wavelengths, we should see a periodic pattern, undergoing one full oscillation between the wavelength λ_1 and λ_2 satisfying the relationship

$$|\beta(\lambda_1) - \beta(\lambda_2)|\Delta L = 2\pi \tag{5}$$

where β depends on wavelength both from the appearance of λ in the denominator of equation 1, but also because the index of refraction of materials (especially the effective index of the photonic waveguide) is wavelength dependent.

We can then approximate equation 5 by assuming that the wavelength difference is small enough that we have

$$(\beta(\lambda_1) - \beta(\lambda_2)) \approx \frac{d\beta}{d\lambda}\Delta\lambda \tag{6}$$

Differentiating equation 1, we have

$$\frac{d\beta}{d\lambda} = 2\pi\left(\frac{dn}{d\lambda}\frac{1}{\lambda} - \frac{n}{\lambda^2}\right) = -\frac{2\pi n_g}{\lambda^2} \tag{7}$$

where we have used the definition of the group index

$$n_g = n - \lambda\frac{dn}{d\lambda} \tag{8}$$

Plugging equations 6 and 7 back into equation 5, we have that the spacing $\Delta\lambda$ corresponding to one full oscillation (the FSR) is

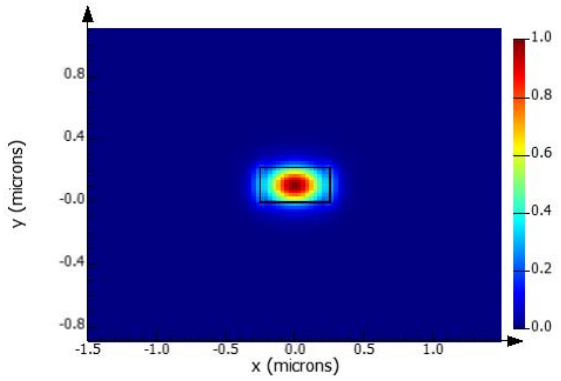

Fig. 1. FDTD simulation of quasi-TE mode of the waveguides used in this work, computed using Lumerical MODE. This image is oriented in a plane perpendicular to the direction of light propagation.

$$FSR = \frac{\lambda^2}{n_g \Delta L} \tag{9}$$

So, if we find the peaks of the spectrum around the wavelength of interest and find the average spacing between them, FSR, we can solve for the group index using the formula

$$n_g = \frac{\lambda^2}{FSR \times \Delta L} \tag{10}$$

We could use equation 10 to calculate the group index from the transmission the spectrum of and MZI, however we will be able to get an even better estimate of the waveguide parameters fitting to the full transfer function in equation 4. We do this to generate a "compact model" of the waveguides in the MZIs and MIs, and compare this with the models that will be computed in section III. Note that the transfer function for the MI is the same as the MZI, but one must take care to account for both passes along the legs of the interferometer to compute the true ΔL.

III. Modeling and simulation

The interferometers were composed of strip waveguides etched into an SOI chip with a 220 nm thick Si layer and a capping oxide layer. The designed widths of the waveguides were 500nm, and light was coupled into the TE mode of the waveguide. This structure can be simulated using the finite difference time domain (FDTD) technique. As an example, the spatial distribution of the waveguide mode from this FDTD simulation is shown in figure 1

One of the essential parameters needed to predict the properties of the MZI is the index of refraction. More specifically, it is important to have an understanding of the effective index of refraction (n_{eff}) which determines the phase velocity of light in the medium. Additionally, if n_{eff} is known as a function of wavelength, it can be used to compute the group index of medium (n_g), which is ultimately the quantity needed to predict the behavior of the MZI. These parameters can be extracted from the FDTD simulation, as shown in figures 2 and 3.

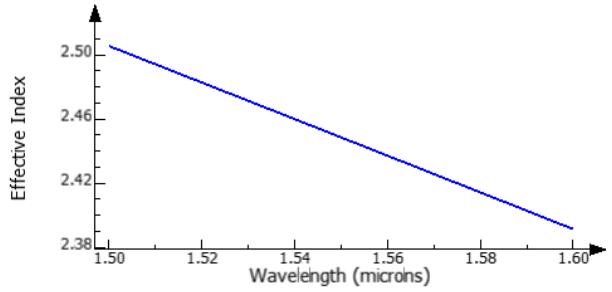

Fig. 2. Variations in the effective index of the proposed waveguide as a function of wavelength. Values are computed from FDTD simulations in Lumerical MODE.

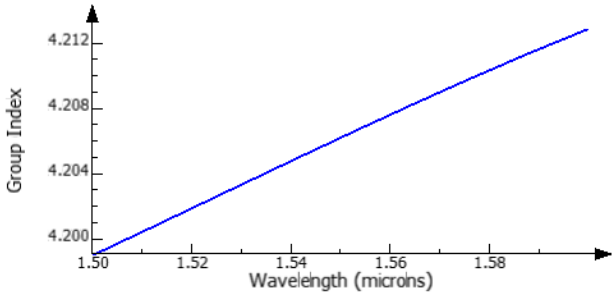

Fig. 3. Variations in the group index of the proposed waveguide as a function of wavelength. Values are computed from FDTD simulations in Lumerical MODE, and are generally in agreement with the simulated effective index.

This information can then be distilled into a compact model for this waveguide by fitting the effective index to a low-order polynomial:

$$n(\lambda) \approx a_0 + a_1(\lambda - \lambda_0) + a_2(\lambda - \lambda_0)^2 \tag{11}$$

Where we arrive at the following fit parameters from the FDTD simulations (for wavelength in units of μm):
$a_0 = 2.4489, a_1 = -1.1337, a_2 = -0.0451$.

Note that if we use this compact model along with equation 8, we find good agreement between the simulated and calculated values of the group index.

Armed with this knowledge, we can now simulate the two proposed devices and see how the simulations compare to the predictions from the equations laid out in section II.

The basic MZI circuit will be composed of Y-branches on the input and output, with each leg of the interferometer composed of a strip waveguide of varying length or width, as shown in figure 4.

We can simulate the behavior of this device in Lumerical INTERCONNECT, as shown in figure 5. We can see the calculated FSR from these simulations are well captured by the transfer function of the MZI (eq 4) and the predicted FSR computed from it (i.e. eq 9), as shown in table I.

The proposed Michelson interferometer is shown in figure 6, where we have used loop waveguides as mirrors and we are using broadband directional couplers to split the light in order to be able to measure the reflected signal. Note the large length imbalance of the two branches.

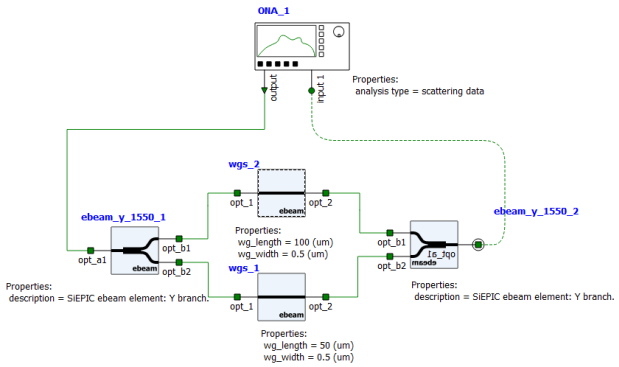

Fig. 4. Proposed schematic of the MZI. As it is drawn, the top waveguide (labelled "wgs_2") is imbalanced in length by 50 μm compared to the bottom waveguide

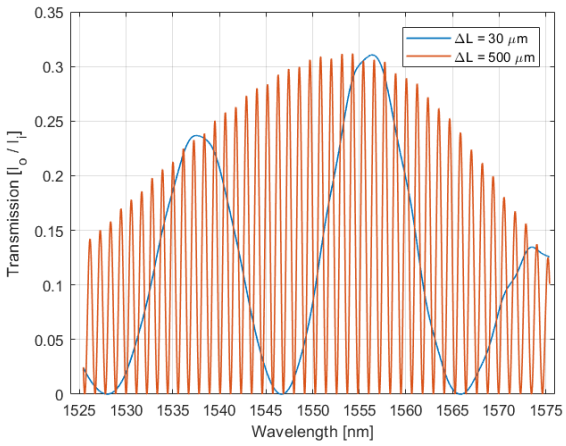

Fig. 5. Simulated transfer function of the MZI device shown in figure 4 for two different length imbalances in the interferometer. Only two of the transfer functions are shown for clarity, the full set of simulations is summarized in table I

Finally, we show the proposed layout for all the devices on this chip in figure 7. This design was built using the SiEPIC PDK and is compact enough to fit into an area of $605\mu m \times 410\mu m$.

IV. Fabrication variability analysis

The above simulations were computed assuming an ideal waveguide that is 500 nm wide and 220 nm thick. In reality, we expect there to be variations from device to device due to imperfections in the thickness of the Si layer in the SOI wafer as well as imperfections in the fabrication of the

$\Delta L(\mu m)$	Calculated FSR (nm)	Simulated FSR (nm)
30	19.040	17.995
50	11.424	11.247
100	5.712	5.682
300	1.904	1.900
500	1.142	1.142

TABLE I

Comparison of the FSR calculated from equation 9 compared to the value extracted from the simulations in Lumerical INTERCONNECT

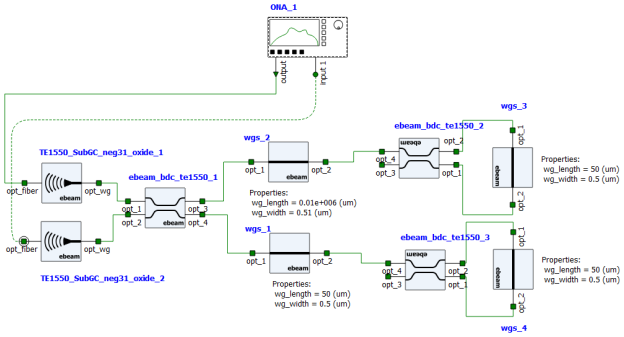

Fig. 6. Schematic of the proposed Michelson interferometer.

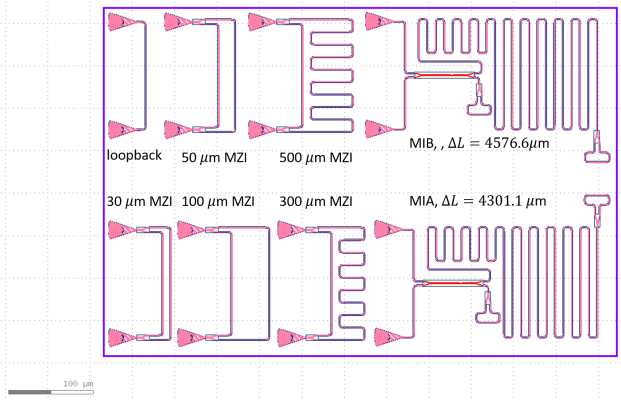

Fig. 7. Layout for the proposed design, including the five Mach-Zehnder interferometers labelled by their length imbalance, the two Michelson interferometers, and a pair of grating couplers connected by a single waveguide to calibrate out the effects of the grating couplers.

waveguide. A corner analysis of the expected variations in waveguide properties as well as device characteristics given an up to 1 standard deviation variation in these parameters is shown in table II. Note that the values of n_{eff} and n_g were computed through FDTD simulation using the specified width and thickness, and the FSR was calculated for a simulated MZI with a length imbalance of 100 μm using the resulting compact model of the waveguide.

V. Final device performance and analysis

To obtain a more precise estimate for n_g, the transmission spectrum of each of the MZIs in the device can be fit to the

width, thickness [nm]	n_{eff}	n_g	FSR [nm]
(nominal) 500, 220.0	2.442	4.177	5.753
470, 215.3	2.371	4.229	5.680
470, 223.1	2.399	4.237	5.665
510, 215.3	2.439	4.159	5.773
510, 223.1	2.466	4.166	5.770

TABLE II

Corner analysis of the effective index, group index, and free spectral range of an MZI with a length imbalance of 100 μm. The variations in thickness are a "worst case scenario" variation, using the the specified 1 standard deviation variability in the Si layer thickness in the SOI wafer from Soitec. The width range is an estimate of the variability in waveguide thickness form past fabrication runs at the SiEPIC foundry.

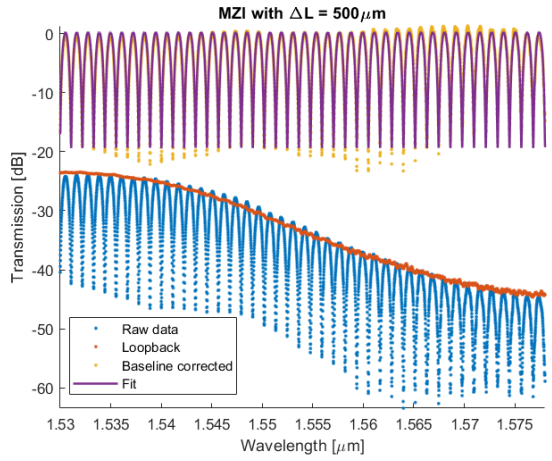

Fig. 8. Fit to the transmission spectrum of the MZI with $\Delta L = 500\mu$m. The loopback data is from two grating couplers connected directly to each other in order to de-embed the losses from the grating couplers themselves. Normalizing the raw data to this envelope results in a tranfer function well-approximated by the fit to equation 4 and a 2nd order compact model for the waveguide index.

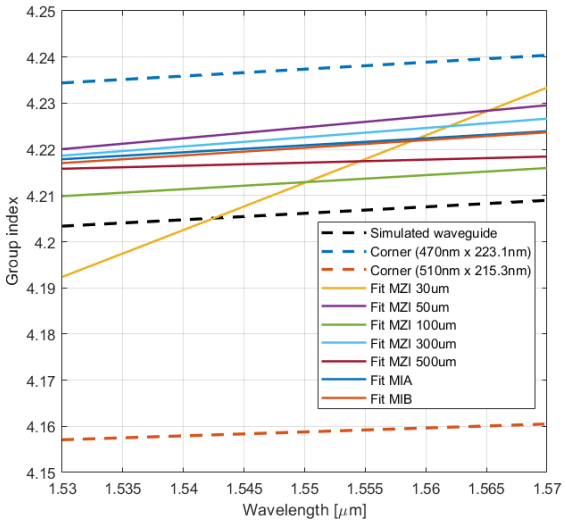

Fig. 9. Fit group index from each of the MZIs listed in table I. The group index from the compact model derived in section III is shown and well as the two curves with the greatest span from the corner analysis in table II as a reference. All fits fall within the range expected from the corner analysis.

functional form of equation 4, where the effective index is parameterized by the compact model described in equation 11. From this compact model, one can compute the group index from equation 8. Using this compact model, we arrive at the following expression for the group index:

$$n_g = a_0 - a_1\lambda_0 + a_2(\lambda_0^2 - \lambda^2) \tag{12}$$

From the fit, we may also extract the parameter uncertainties for the a_i coefficients, σ_{a_i}. We can then propagate error through equation 12 via

$$\sigma_{n_g}^2 = \sum_i \sigma_{a_i}^2 \left(\frac{\partial n_g}{\partial a_i}\right)^2 \tag{13}$$

arriving at the expression for the (1σ) uncertainty in the group index:

$$\sigma_{n_g} = \sqrt{\sigma_{a_0}^2 + \sigma_{a_1}^2\lambda_0^2} \tag{14}$$

An example of one of the fits to the MZI transmission spectrum is shown in figure 8. The calculated compact model from each of the interferometers in the device is shown in figure 9. The fit parameters and uncertainties as well as the resulting fit and uncertainties in n_g and FSR are shown in table III. In general, we find precise estimates for the group index that are generally in agreement with each other, though the device-to-device variation seems to be higher than the fit uncertainties. We also note to good agreement between the measured FSR and the simulated and calculated values listed in table I.

ΔL [μm]	a_0	$a_1[\mu\text{m}^{-1}]$	$a_2[\mu\text{m}^{-2}]$	n_g	FSR [nm]
30	2.44731(2)	-1.1390(7)	-0.33(4)	4.2127(9)	19(1)
50	2.450678(6)	-1.1446(2)	-0.08(2)	4.2248(3)	11.3(4)
100	2.457414(5)	-1.1326(2)	-0.05(1)	4.2129(2)	5.71(3)
300	2.457878(2)	-1.13855(6)	-0.065(4)	4.22262(7)	1.90(2)
500	2.4620610(9)	-1.13229(4)	-0.021(4)	4.21711(6)	1.14(3)
4301.12	2.4698835(2)	-1.12967(3)	-0.049(5)	4.22087(3)	0.132(6)
4576.60	2.4695804(2)	-1.12952(2)	-0.054(4)	4.22034(2)	0.124(5)
average	2.459(9)	-1.135(6)	-0.1(1)	4.219(5)	-

TABLE III

SUMMARY OF THE FIT PARAMETERS AND GROUP INDEX FROM THE INTERFEROMETERS CONSIDERED IN THIS WORK. THE 1σ UNCERTAINTY IS LISTED IN PARENTHESES AFTER THE LAST SIGNIFICANT DIGIT. FOR THE FIT PARAMETERS FOR EACH DEVICE, THIS VALUE IS THE UNCERTAINTY RESULTING FROM THE FIT ALONE, WHEREAS THE UNCERTAINTY LISTED IN THE **AVERAGE** ROW IS THE STANDARD DEVIATION OF THE VALUES IN EACH COLUMN. THE GROUP INDEX n_g IS REPORTED AT 1550 NM. THE FSR AND CORRESPONDING UNCERTAINTY IS THE AVERAGE AND STANDARD DEVIATION OF THE PEAKS BETWEEN 1540 AND 1560 NM WITH THE EXCEPTION OF THE 30 AND 50 μM DEVICES, WHICH INCLUDE DATA BETWEEN 1500 AND 1580 NM IN INCREASE STATISTICS

VI. FUTURE WORK

This work established the technique to measure the group index of fabricated waveguides using interferometry. There are a few extensions to this work that would improve the results. In this work, the transfer function of each interferometer is fit separately and any loss beyond that caused by the grating couplers is normalized to unity transmission via a free "device loss" parameter in the model. This was needed because the loopback to calibrate the losses in the waveguide were not completely representative of all the losses in the system (for instance, through Y-branches). However, it is likely that there is a uniquely identifiable loss from each component as well as absorption in the waveguides themselves. These parameters could be determined through more independent measurements of the individual components to calibrate out that loss, and a simultaneous fit on the MZI transfer functions to fit a single absorption loss in the waveguides. Additionally, the use of longer ΔL and more stable lasers would be able to increase the precision of these fits. Finally, testing of more identical devices would yield a better estimate of the variation due to fabrication imperfections alone.

VII. Fabrication and measurement

The photonic devices were fabricated using the NanoSOI MPW fabrication process by Applied Nanotools [2] which is based on direct-write 100 keV electron beam lithography technology. Silicon-on-insulator wafers of 200 mm diameter, 220 nm device thickness and 2 μm buffer oxide thickness are used as the base material for the fabrication. The wafer was pre-diced into square substrates with dimensions of 25x25 mm, and lines were scribed into the substrate backsides to facilitate easy separation into smaller chips once fabrication was complete. After an initial wafer clean using piranha solution (3:1 H_2SO_4:H_2O_2) for 15 minutes and water/IPA rinse, hydrogen silsesquioxane (HSQ) resist was spin-coated onto the substrate and heated to evaporate the solvent. The photonic devices were patterned using a Raith EBPG 5000+ electron beam instrument using a raster step size of 5 nm. The exposure dosage of the design was corrected for proximity effects that result from the backscatter of electrons from exposure of nearby features. Shape writing order was optimized for efficient patterning and minimal beam drift. After the e-beam exposure and subsequent development with a tetramethylammonium sulfate (TMAH) solution, the devices were inspected optically for residues and/or defects. The chips were then mounted on a 4" handle wafer and underwent an anisotropic ICP-RIE etch process using chlorine after qualification of the etch rate. The resist was removed from the surface of the devices using a 10:1 buffer oxide wet etch, and the devices were inspected using a scanning electron microscope (SEM) to verify patterning and etch quality. A 2.2 μm oxide cladding was deposited using a plasma-enhanced chemical vapour deposition (PECVD) process based on tetraethyl orthosilicate (TEOS) at 300^{o}C. Reflectrometry measurements were performed throughout the process to verify the device layer, buffer oxide and cladding thicknesses before delivery.

To characterize the devices, a custom-built automated test setup [1], [3] with automated control software written in Python was used [4]. An Agilent 81600B tunable laser was used as the input source and Agilent 81635A optical power sensors as the output detectors. The wavelength was swept from 1500 to 1600 nm in 10 pm steps. A polarization maintaining (PM) fiber array was used to couple light in/out of the chip [5]. This maintained the polarization state of the light to couple the TE polarization into the grating couplers [6].

Acknowledgments

I acknowledge the edX UBCx Phot1x Silicon Photonics Design, Fabrication and Data Analysis course, which is supported by the Natural Sciences and Engineering Research Council of Canada (NSERC) Silicon Electronic-Photonic Integrated Circuits (SiEPIC) Program. The devices were fabricated by Cameron Horvath at Applied Nanotools, Inc. Hossam Shoman performed the measurements at The University of British Columbia. I acknowledge Lumerical Solutions, Inc., Mathworks, Mentor Graphics, Python, and KLayout for the design software.

References

[1] L. Chrostowski and M. Hochberg, *Silicon Photonics Design: From Device to System*. Cambridge University Press, 2015.
[2] "Applied Nanotools Inc.." http://www.appliednt.com/nanosoi. Edmonton, Canada.
[3] "Maple Leaf Photonics." http://mapleleafphotonics.com. Seattle WA, USA.
[4] https://siepic.ca/fabrication/. using Python code developed by Michael Caverley.
[5] "PLC Connections." www.plcconnections.com. Columbus OH, USA.
[6] Y. Wang, X. Wang, J. Flueckiger, H. Yun, W. Shi, R. Bojko, N. A. F. Jaeger, and L. Chrostowski, "Focusing sub-wavelength grating couplers with low back reflections for rapid prototyping of silicon photonic circuits," *Optics Express*, vol. 22, no. 17, p. 20652, 2014.